An Approximate Unsteady Aerodynamic Model for Flapped Airfoils Including Improved Drag Predictions

Li Liu
Postdoctoral Researcher
ryanliu@umich.edu

Peretz P. Friedmann
François-Xavier Bagnoud
Professor of Aerospace Engineering
peretzf@umich.edu

Ashwani K. Padthe
Ph.D. Candidate
akpadthe@umich.edu

Department of Aerospace Engineering
University of Michigan, Ann Arbor, Michigan

Abstract

Actively controlled trailing-edge flaps (ACFs) have been extensively studied for vibration and noise control in rotorcraft using various approximate aerodynamic models. In this study, two-dimensional unsteady airloads due to oscillating flap motion obtained from computational fluid dynamics (CFD) are compared with approximate unsteady loads. The approximate loads are obtained from the Rational Function Approximation (RFA) model developed for use with comprehensive rotorcraft simulation codes, which is a state-space, time-domain model that accounts for unsteadiness, compressibility and time-varying freestream effect. Unsteady compressible Reynolds-averaged Navier-Stokes computations are based on an overset mesh that accounts for oscillatory flap motion. The comparison is conducted over a wide range of unsteady flow conditions representing combinations of parameters such as airfoil angle of attack, flap deflection amplitudes, reduced frequencies, and freestream Mach numbers. The comparison between the RFA model and CFD based calculations illustrates the limitations of the approximate theory, particularly at transonic Mach numbers and high angles of attack where nonlinear effects dominate. Nevertheless, the RFA model yields a good approximation for the unsteady effects of the blade section/trailing edge flap combination, for conditions representative of rotorcraft aerodynamic environment. An improved drag model for flapped airfoils is developed using surrogate based approximation. This new drag model can be implemented in comprehensive rotorcraft simulation codes to predict performance penalty associated with active flap deflections.

Nomenclature

A	Amplitude of flap deflection
b	Airfoil semi-chord $= c/2$
c	Airfoil chord
$\mathbf{C}_0, \mathbf{C}_1, ..., \mathbf{C}_{n+1}$	Rational function coefficient matrices
C_l	Lift coefficient
C_m	Moment coefficient
C_{hm}	Hinge moment coefficient
C_d	Total drag coefficient
D_0, D_1	Generalized flap motions
$\mathbf{D}, \mathbf{E}, \mathbf{R}$	Matrices defined in the RFA model
$f(\mathbf{x})$	Function for global behavior in kriging
$\mathbf{f}$	Generalized load vector
$\mathbf{G}$	Laplace transform of $\mathbf{f}(\bar{t})U(\bar{t})$
$\mathbf{h}$	Generalized motion vector
$\mathbf{H}$	Laplace transform of $\mathbf{h}(\bar{t})$
k	Reduced frequency $= 2\pi\nu b/U$
M	Mach number
n_L	Number of lag terms
N_{tp}	Number of test points
$\bar{p}$	Nondim. surface pressure distribution
$\mathbf{Q}$	Aerodynamic transfer function matrix
$\tilde{\mathbf{Q}}$	Approximation of $\mathbf{Q}$
s	Laplace variable

1

$\bar{s}$	Nondim. Laplace variable $= sb/U$
t	Time
$\bar{t}$	Reduced time $= \frac{1}{b}\int_0^t U(\tau)d\tau$
$U(t)$	Freestream velocity, time-dependent
W_0, W_1	Generalized airfoil motions
$\mathbf{x}(t)$	Aerodynamic state vector
$y(\mathbf{x})$	Unknown function to be approximated
$\bar{y}$	Mean response value for all test points
$y^{(i)}$	Direct CFD results at i^{th} test point
$\hat{y}^{(i)}$	Surrogate prediction at i^{th} test point
$Z(\mathbf{x})$	Stochastic realization in kriging
α	Airfoil angle of attack
γ_n	Rational approximant poles
δ_e	Flap deflection angle
$\Delta\mathrm{C}_{d,\text{flap}}$	Additional drag due to flap deflection
$\Delta\mathrm{C}_l, \Delta\mathrm{C}_m, \Delta\mathrm{C}_{hm}, \Delta\mathrm{C}_d$	Half peak-to-peak values of unsteady force coefficients
ν	Frequency of flap oscillation in Hz
$\bar{\omega}$	Nondim. normal velocity distribution

Introduction and Background

With the advent of actively controlled trailing edge flaps (ACFs) as a viable control device for vibration and noise reduction in helicopters [1–9], the ability to accurately model aerodynamic effects due to unsteady flap motion has gained importance. The first studies on ACFs have employed classical quasisteady Theodorsen type aerodynamics to represent the effect of the flaps for active vibration reduction [3]. Subsequently, more refined aerodynamic models were developed for use in comprehensive rotorcraft simulation codes, as the importance of unsteadiness, compressibility, as well as time-varying freestream effects in rotorcraft was recognized. An example of such models is that developed by Leishman based on indicial aerodynamics [10]. Approximate unsteady airloads due to arbitrary airfoil and flap motion were obtained via Duhamel superposition integral using Wagner's indicial response functions. This model accounts for compressibility and can be extended to time-varying freestreams. The Leishman model has been incorporated in a comprehensive rotorcraft code (UMARC).

The Rational Function Approximation (RFA) approach is an effective approach, developed for fixed wing applications, for generating a Laplace transform or state variable representation of the unsteady aerodynamics of a wing section [11–14]. Myrtle and Friedmann used this approach to develop an unsteady compressible aerodynamic model based on the RFA approach that also accounts for time-varying freestream effects, and is suitable for rotary wing applications where one needs to represent a two-dimensional blade section or blade section/trailing-edge flap combination [5]. An advantage of such an aerodynamic model is its compatibility with equations with periodic coefficients that govern the rotary wing aeroelastic problem in forward flight. The principal advantages of the RFA model are: 1) it facilitates the combination of the aerodynamics with the structural dynamic model; 2) it yields a solution procedure of the combined system based on numerical integration; and 3) it affords a degree of computational efficiency required by the implementation of active control techniques such as trailing edge flaps. The RFA model has been implemented in a comprehensive rotorcraft simulation code, called AVINOR (for active vibration and noise reduction), used in several computational studies demonstrating the effectiveness of active flaps on helicopter vibration and noise reduction, as well as performance enhancement [5, 6, 8, 15, 16]. The RFA model has been extended to compute chordwise pressure distribution that are required for aeroacoustic computations, and it has produced results which correlate well with experimental data [8, 17].

Correlation studies in which results from the comprehensive rotorcraft simulation code using the RFA aerodynamics [6, 17] have shown that despite its relative simplicity the RFA model produces good agreement with experimental data. Ideally the accuracy of RFA aerodynamics for blade/flap combination should be validated by comparison with experimental data. However, experimental data on blade and oscillating flap combinations are not available. Therefore, a viable alternative is to generate data for effect of unsteady flaps using a CFD based approach. Such an approach allows direct comparisons between RFA and CFD based aerodynamics for any flow conditions and active flap configurations that are representative of rotorcraft applications.

The last two decades have produced remarkable improvements in algorithms and techniques suitable for unsteady flow simulations. These advances combined with rapid increases in computing power allow one to conduct Navier-Stokes simulations of time-dependent flowfields around complex geome-

tries including the effect of various flow control devices. A fairly comprehensive overview of the capabilities and limitations of current unsteady CFD approaches for active flow control was provided in Ref. 18. Among the various approaches, unsteady Reynolds-averaged Navier Stokes (RANS) equations have been used to simulate a broad range of time-dependent turbulent flows, by taking advantage of the reduced computational cost at high Reynolds numbers. Furthermore, the RANS based CFD results have shown good agreement with experiments for many different types of unsteady flow problems, including those involving unsteady leading-edge or trailing-edge control surfaces [19]. It should be noted that the time-averaging nature of the methodology can encounter difficulties when dealing with massively separated flows. Furthermore, the approach requires a turbulence model that has to be selected from a number of available turbulence models, and in some cases different turbulence models can produce significantly different results. In Ref. 19, pressure distributions on a wing surface with a statically or dynamically deflected spoiler and aileron were calculated at a Mach number of M=0.77, using two compressible RANS codes, CFL3DAE and ENS3DAE. The computational results were compared to test data obtained from the Benchmark Active Control Technology (BACT) program at NASA Langley [20]. Deforming mesh option was used to simulate the oscillatory aileron motion, and a continuous surface approach was employed where the hinge gap of the aileron was neglected. The CFD based results obtained reasonably good agreement with the experiments, for both steady and unsteady cases. Another study [21] compared unsteady pressure distributions obtained for the BACT wing due to trailing-edge flap deflection, using the CFL3D code with a doublet lattice method (DLM) solution. The overall pressure distributions obtained by DLM produced acceptable correlation and outperformed the CFD predictions near the hingeline. This was attributed to inadequate meshing in the vicinity of the hinge. The pressure predictions by DLM were less accurate on the control surface, near the airfoil leading edge and around the shock regions, due to the limitations of the linear potential theory.

The actively controlled flaps, used for vibration or noise reduction, may incur a performance penalty due to the unsteady drag associated with flap deflection, a cause for concern when the practical use of an ACF device is sought. Thus, the estimation of this drag penalty is important. An approximate drag correction due to flap deflections based on limited experimental data was obtained in Ref. 15. However, this approximate model has not been validated by comparing it to CFD data. Accurate unsteady drag prediction on a blade/oscillating flap combination by CFD is a fairly complex task which is affected by several factors such as mesh sizing and turbulence models [22]. Recent experience with drag predictions for three-dimensional wing and wing-body configurations [23] suggests that drag obtained based on current CFD methodologies is useful.

The principal objectives of this paper are: (a) to provide a careful comparison of the approximate RFA unsteady aerodynamic model with CFD based results for lift and moment, and (b) to provide a good approximation to unsteady drag on an airfoil/oscillating flap combination. The specific objectives of the paper are:

1. Compare two-dimensional unsteady lift, moment and hinge moment obtained from the RFA model to CFD computations, on an airfoil with an oscillating trailing-edge flap;

2. Determine the effect of compressibility and oscillating flap reduced frequencies for a practical range of flap motions and free stream Mach numbers that are representative of rotorcraft applications;

3. Compare aerodynamic drag due to flap obtained from CFD computations with a simplified drag model, used in earlier research [15];

4. Develop an improved drag model based on CFD results, suitable for use with comprehensive rotorcraft simulation codes for performance enhancement studies.

These goals constitute a valuable contribution to the fundamental understanding of the aerodynamics of airfoils equipped with oscillating trailing edge flaps, and at the same time serve as a validation of the approximate RFA model. Furthermore, an improved drag model is essential for accurate assessment of the ACF approach for rotor performance enhancement.

Concise Description of the RFA Model

The RFA model developed in Ref. 5 is based on Roger's approximation [11] for representing aerody-

namic loads in the Laplace domain

$$\mathbf{G}(\bar{s}) = \mathbf{Q}(\bar{s})\mathbf{H}(\bar{s}), \qquad (1)$$

where $\mathbf{G}(\bar{s})$ and $\mathbf{H}(\bar{s})$ represent Laplace transforms of the generalized aerodynamic load and generalized motion vectors, respectively. The aerodynamic transfer matrix $\mathbf{Q}(\bar{s})$ is approximated using the Least Squares approach with an expression of the form

$$\tilde{\mathbf{Q}}(\bar{s}) = \mathbf{C}_0 + \mathbf{C}_1\bar{s} + \sum_{n=1}^{n_L} \frac{\bar{s}}{\bar{s} + \gamma_n}\mathbf{C}_{n+1}. \qquad (2)$$

where Eq. (2) is usually denoted Roger's approximation. The n_L terms in the summation are aerodynamic lag terms associated with a number of poles γ_n. These poles are assumed to be positive valued to produce stable open loop roots, but are otherwise not critical to the approximation. The arbitrary motions of the airfoil and the flap are represented by four generalized motions depicted in Figure 1. The normal velocity distributions shown in Figure 1 correspond to two generalized airfoil motions, denoted by W_0 and W_1, and two generalized flap motions, denoted by D_0 and D_1. In order to find the Least Squares approximant for the aerodynamic response, tabulated oscillatory airloads, i.e. sectional lift, moment and hinge moment, need to be obtained corresponding to the four generalized motions. The oscillatory airloads in the frequency domain are obtained from a two-dimensional doublet lattice method (DLM) solution [24] of Possio's integral equation [25] which relates pressure $\bar{p}$ to surface normal velocity $\bar{w}$ as shown below in Eq. (3)

$$\bar{w}(x) = \frac{1}{8\pi}\int_{-1}^{1} \bar{p}(\zeta)K(M, x - \zeta)d\zeta, \qquad (3)$$

where K is the kernel function. This approach is suitable for generating efficiently a set of aerodynamic response data for the airfoil/flap combination. The frequency domain information is generated for an appropriate range of reduced frequencies and Mach numbers.

The state space representation of the RFA aerodynamic model requires a generalized motion vector $\mathbf{h}$ and a generalized load vector $\mathbf{f}$, defined as:

$$\mathbf{h} = \begin{bmatrix} W_0 \\ W_1 \\ D_0 \\ D_1 \end{bmatrix} \quad \text{and} \quad \mathbf{f} = \begin{bmatrix} C_l \\ C_m \\ C_{hm} \end{bmatrix}. \qquad (4)$$
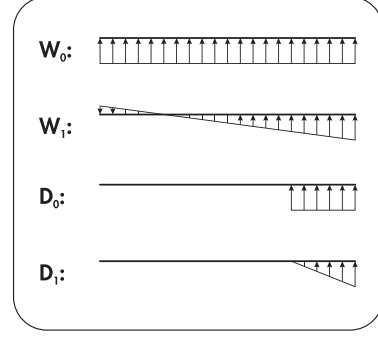

Figure 1: Normal velocity distribution corresponding to generalized airfoil and flap motions.

The Laplace transform representation in Eq. (1) is related to the generalized motion and generalized forces, through the following expressions

$$\mathbf{G}(\bar{s}) = \mathcal{L}[\mathbf{f}(\bar{t})U(\bar{t})] \quad \text{and} \quad \mathbf{H}(\bar{s}) = \mathcal{L}[\mathbf{h}(\bar{t})] \qquad (5)$$

where $U(\bar{t})$ is the time-dependent free stream velocity. Here the reduced time $\bar{t}$ is defined such that unsteady freestream effects can be properly accounted for [5], and may be interpreted as the distance measured in semi-chords. The rational approximant $\tilde{\mathbf{Q}}$ in Eq. (2) can be transformed to the time domain using the inverse Laplace transform, which yields the final form of the state space model, given below

$$\dot{\mathbf{x}}(t) = \frac{U(t)}{b}\mathbf{R}\mathbf{x}(t) + \mathbf{E}\dot{\mathbf{h}}(t), \qquad (6)$$

$$\mathbf{f}(t) = \frac{1}{U(t)}\left(\mathbf{C}_0\mathbf{h}(t) + \mathbf{C}_1\frac{b}{U(t)}\dot{\mathbf{h}}(t) + \mathbf{D}\mathbf{x}(t)\right). \qquad (7)$$

where the matrices $\mathbf{D}$, $\mathbf{R}$ and $\mathbf{E}$ are given by

$$\mathbf{D} = \begin{bmatrix} \mathbf{I} & \mathbf{I} & \dots & \mathbf{I} \end{bmatrix}, \quad \mathbf{R} = -\begin{bmatrix} \gamma_1\mathbf{I} & & & \\ & \gamma_2\mathbf{I} & & \\ & & \dots & \\ & & & \gamma_{n_L}\mathbf{I} \end{bmatrix},$$

$$\mathbf{E} = \begin{bmatrix} \mathbf{C}_2 \\ \mathbf{C}_3 \\ \vdots \\ \mathbf{C}_{n_L+1} \end{bmatrix}.$$

Concise Description of the CFD Flow Solver

The CFD results generated in this study are obtained using the CFD++ package [26, 27] developed by METACOMP Technologies. The CFD++

4

code is a modern versatile tool capable of solving the compressible unsteady Reynolds-averaged Navier-Stokes equations using a finite volume formulation. The code has several advanced features such as Large Eddy Simulation (LES) and hybrid LES/RANS models. The CFD++ code supports a variety of operating systems and multiple parallel clusters, with input and output files compatible across all platforms. It also provides a user-friendly graphical interface for convenient problem setup. An important feature of the code is a unified grid methodology that can handle a variety of structured, unstructured, multi-block, and hybrid meshes, including patched and overset grid capabilities. Various cell types can be used within the same mesh, such as hexahedral, triangular prism, pyramid and tetrahedral elements in 3-D, quadrilateral and triangular elements in 2-D, and line elements in 1-D. Spatial discretization is based on a second order multi-dimensional Total Variation Diminishing (TVD) scheme. For temporal scheme an implicit algorithm with dual time-stepping is employed to perform time-dependent flow simulations, with a multi-grid acceleration option for subiterations. Various turbulence models are available in CFD++, ranging from one to three-equation transport models. The Spalart-Allmaras (S-A) turbulence model [28] is chosen for the current study, and a fully turbulent boundary layer is assumed.

To simulate unsteady flap deflection, an overset mesh option is employed where a separate body-fitted mesh for the trailing-edge flap is generated in addition to the airfoil mesh, as illustrated in Fig. 2. An overset grid approach is convenient for modeling arbitrarily large grid motions; however, non-conservation of flow variables at the grid zonal interfaces may affect the solution accuracy [29]. Sinusoidal flap motions about the hinge axis can be prescribed in the CFD++ code. The relative motion of the two grids requires re-computation of overset boundary zonal connections at each time step, which is executed automatically by the code.

Drag Models for Flapped Airfoils

The RFA model, which is based on potential flow theory, has no provision for drag calculation. However, accurate drag predictions are needed to assess performance penalty due to active flaps. A simple drag correction that accounts for additional drag due to flap deflections has been suggested in Ref. 15,
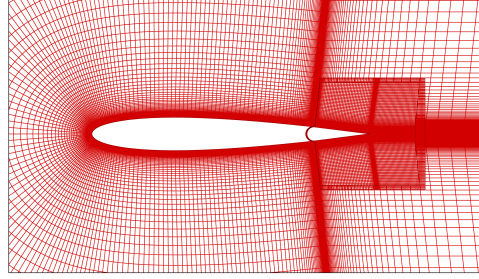

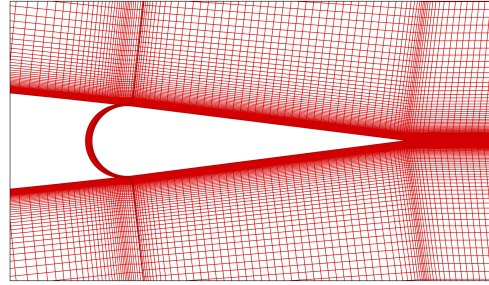Figure 2: Overset grid on a NACA0012 airfoil.

Figure 3: Gap between the airfoil and the flap sections of the geometry.

using static experimental data in a quasi-static manner. In this study, the model will be validated by comparing this approximate model with CFD computations. Furthermore, a new approximate drag model is also developed using CFD drag data, by employing surrogate based approximation method. The resulting reduced order drag model is capable of providing the degree of computational efficiency required by helicopter simulations, while taking advantage of the accuracy afforded by advanced CFD techniques.

Simple drag model

The additional drag due to deflection of a 20% plain flap is given by the following approximate equation [15]

$$\Delta C_{d,\text{flap}} = 0.001|\delta_e| \qquad (8)$$

This drag model has been used in our helicopter simulations to estimate the effect of active flaps on rotor performance.

Surrogate drag model

Combining a comprehensive rotorcraft simulation with a CFD code in order to carry out active control studies for vibration reduction would incur prohibitive computational costs. Therefore, surrogate based approximation techniques are employed to construct a reduced order drag model. Surrogate methods replace the "true" function with a smooth functional relationship of acceptable accuracy that can be evaluated quickly.

In order to construct the surrogates, the unknown function must first be evaluated over a set of design points. The surrogate is then generated by fitting the initial design points. Drag for a two dimensional airfoil/flap combination is first evaluated over a set of specified flow conditions, characterized by three flow variables, or design variables for the drag surrogate. These variables are: freestream Mach number M, airfoil angle of attack α, and flap deflection angle δ_e. Note that the choice of these three design variables implies a quasisteady drag model for flapped airfoils. Subsequently, the surrogate is generated by fitting the drag data over these flow conditions.

The kriging interpolation technique is used to generate the surrogate drag model, because this technique has been shown to perform well when fitting highly nonlinear functions [30, 31]. In kriging, the unknown function $y(\mathbf{x})$ is assumed to be of the form

$$y(\mathbf{x}) = f(\mathbf{x}) + Z(\mathbf{x}) \qquad (9)$$

where $f(\mathbf{x})$ is an assumed function (usually polynomial form) and $Z(\mathbf{x})$ is a realization of a stochastic (random) process which is assumed to be Gaussian. The function $f(\mathbf{x})$ can be thought of as a global approximation of $y(\mathbf{x})$, while $Z(\mathbf{x})$ accounts for local deviations which ensure that the kriging model interpolates the data points exactly. In this study, $Z(\mathbf{x})$ is based on Gaussian spatial correlation functions, and $f(\mathbf{x})$ is assumed to be a second order polynomial. Maximum likelihood estimation is used to select the fitting parameters [32, 33]. The kriging surrogates were created with a MATLAB kriging toolbox, which is free software [34].

Results and Discussions

The results presented in this section are for a NACA0012 airfoil with an oscillating trailing edge flap. The airfoil has a chord with a dimensional value of $c = 0.1m$, and the flap has a chord of 0.20c
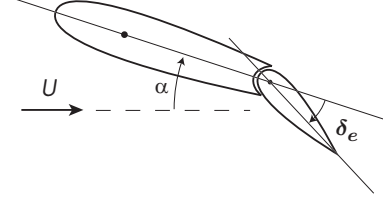

Figure 4: Airfoil with a trailing-edge flap.

and is hinged at the 0.80c location. These dimensions are chosen to match the experimental studies described in Ref. 35. A hinge gap of 0.01c is modeled as shown in Fig. 3. The simulations were carried out for two mean airfoil angles of attack, $\alpha = 0°$ and 5°, respectively. The majority of the results are for a specific Mach number $M = 0.6$, unless otherwise stated. Additional calculations were conducted at various free stream Mach numbers ranging from low subsonic to transonic to study the effect of Mach numbers. The Reynolds number is 4.86×10^6 based on airfoil chord. The unsteady flap motion is given by Eq. (10),

$$\delta_e = A\sin(2\pi\nu t) = A\sin(k\bar{t}) \qquad (10)$$

where k is the reduced frequency. The geometry of the airfoil/flap configuration is shown in Fig. 4.

The domain for the CFD computations is depicted in Fig. 5, and the far field boundary extends to 50 chord lengths. The details of the grid near the airfoil and the flap are given in Figs. 2 and 3. The grids for the airfoil and the flap are structured grids with quadrilateral elements, generated using the ICEM-CFD software and converted into the native format in CFD++. The grids are refined at the solid wall boundaries so that the equations are directly solved to the walls and wall functions are not used. Two grids representing different levels of mesh resolution are generated for grid convergence studies. A medium resolution grid contains 90,000 grid points, as shown in Figs. 2, 3 and 5; while the finer grid has 244,000 points. The flow is first allowed to reach steady state, before the time-dependent results due to flap deflections are generated using the overset mesh approach that was described earlier. The time-accurate simulations utilize time steps such that at least 250 points are used per cycle. The computational cost of the CFD simulations was approximately 1 hour for each cycle on the medium grid and over 2 hours on the finer grid, using four CPUs on a Linux cluster of Opteron processors with speeds of 1.8–2.4GHz.
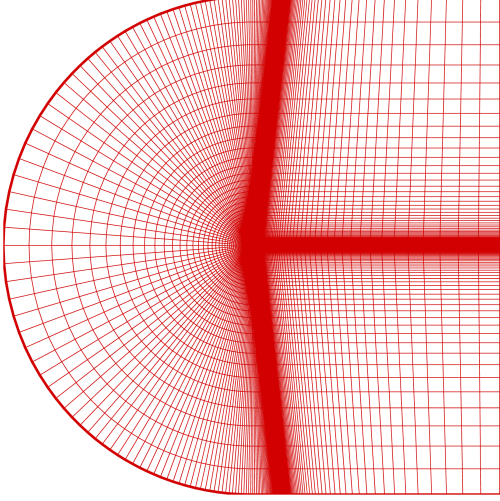
Figure 5: Grid for a NACA0012 airfoil with flap
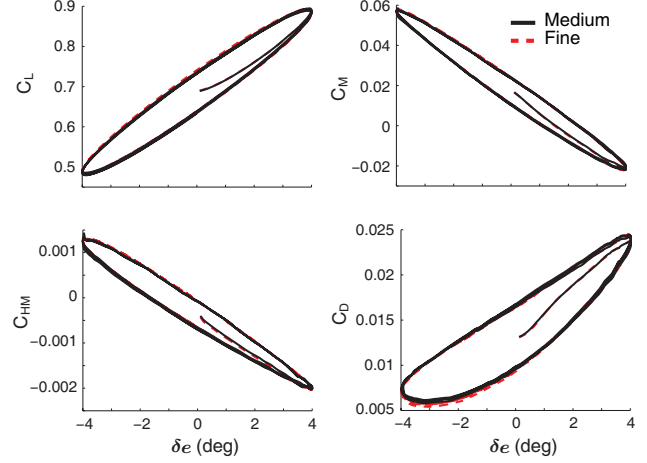

Figure 6: Comparison of force coefficients with the medium and fine grids; $A = 4°$, $k = 0.0624$, M = 0.6 and $\alpha = 5°$.

The results presented are organized in the following manner. First, a grid sensitivity study is conducted on the medium and fine grids. Next, unsteady values of the lift coefficient C_l, moment coefficient C_m, and hinge moment coefficient C_{hm} due to oscillatory flap motion are presented, comparing the RFA and the CFD results. Note that the moment coefficient C_m is defined about the quarter chord point, and the hinge moment C_{hm} is measured about the hinge axis. The effects of freestream Mach number on predicted unsteady airloads are also discussed by comparing the RFA and CFD results. Subsequently, the drag coefficient C_d is compared for the CFD and approximate drag models.

Grid convergence

The sensitivity of CFD calculations to grid resolution is considered first, shown in Fig. 6. Lift, moment, hinge moment and drag coefficients versus flap deflection are shown for the case where airfoil incidence $\alpha = 5°$ and the flap deflection magnitude $A = 4°$, for the medium and fine grids. The simulations on the two grids produced very similar results, as evident from Fig. 6, which implies low sensitivity to grid resolution for the particular case considered. Based on this comparison, the medium grid is deemed to be adequate for resolving the flow features and will be used for the results presented in this section.

Unsteady lift, moment and hinge moment

To study the effect of oscillating flap on unsteady airloads, pressure contours are first shown in Fig. 7 at four instantaneous flap deflection angles during one oscillatory cycle, i.e. at $\delta_e = 0°, 4°, 0°$ and $-4°$. The flap reduced frequency is 0.0624 and flap deflection amplitude $A = 4°$. Unsteady flap motion clearly has a significant effect on overall pressure distribution as can be seen from the variation of the pressure contours during the cycle.
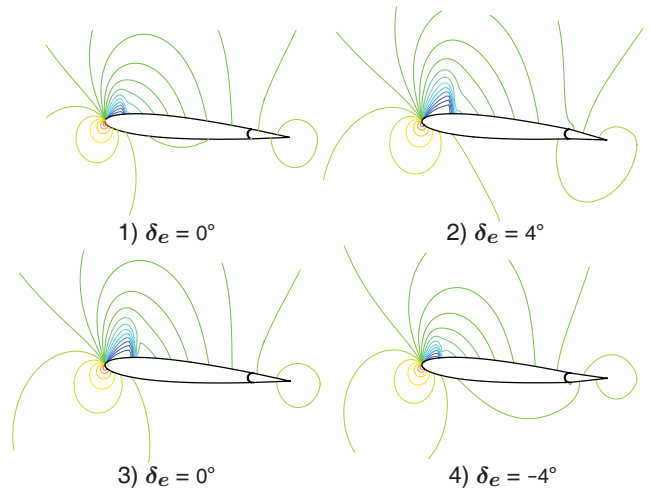

Figure 7: Pressure contours at four instantaneous flap angles; $A = 4°$, $k = 0.0624$, M = 0.6 and $\alpha = 5°$.

Next, results from the CFD are obtained and compared to the RFA model, for flow conditions

representative of practical active flap applications. Typical active flap frequencies used for noise and vibration control on a four-bladed helicopter rotor are in the range of 2-5/rev, which correspond to reduced frequencies of approximately 0.05–0.20. Therefore, unsteady airloads are generated for flap frequencies $\nu = 20, 40, 80, 120$ Hz, corresponding to reduced frequencies between 0.031–0.187, at freestream Mach number of 0.6.

The time history of the lift coefficient C_l is shown in Figure 8, for 2° flap deflection. Figure 8 implies that the RFA model consistently overpredicts the unsteady lift compared to the CFD results by approximately 20-30% at all four frequencies. The same lift coefficient data is also plotted versus flap deflection angle δ_e, and is given in Fig. 9. The characteristic loops in Fig. 9 are indicative of a time lag, which is similar for the RFA and CFD results.

The unsteady lift due to the flap motion at zero airfoil incidence $\alpha = 0°$ is presented in Figs. 10 and 11 to serve as a comparison to the earlier results presented for $\alpha = 5°$. The results display the same trends that have been noted for the case with an incidence of $\alpha = 5°$, which implies that the trends observed are not sensitive to the incidence setting on the airfoil.

The oscillatory portion of C_l, denoted by ΔC_l, due to flap deflection amplitudes of $A = 2°$ and $4°$, is compared in Fig. 12. Figure 12 indicates that the difference in ΔC_l between the RFA and CFD predictions increase as the flap deflection angle increases. This behavior is reasonable since the nonlinear flow effects are enhanced as the flap deflections increase. Similar to the 2° case, the RFA model overestimates ΔC_l at 4° as compared to the results generated from the CFD code. Generally, the amplitudes of ΔC_l diminish as the flap oscillation frequency ν increases, reflecting the unsteady effect of the flap. This trend is captured by both the RFA model and CFD results. However, ΔC_l predicted by the CFD code starts to increase slightly at frequencies above 80Hz. The maximum error in ΔC_l is 45% and the minimum error is 21%, for the cases considered here.

The pitching moment coefficients C_m are shown next for an airfoil incidence of $\alpha = 5°$ and flap amplitude of 2°. The variation in C_m is plotted versus time in Fig. 13, and subsequently C_m versus flap deflection angle is shown in Fig. 14. There is a substantial difference between the average values of C_m predicted by the RFA and the CFD code as evident from the figures. The value of C_m obtained from the RFA model oscillates about zero, whereas C_m from
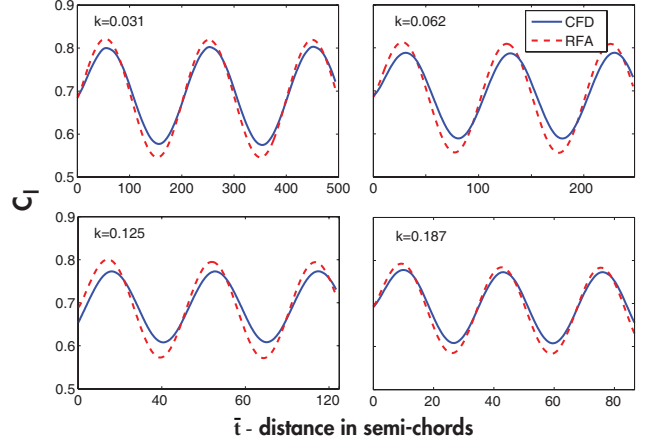

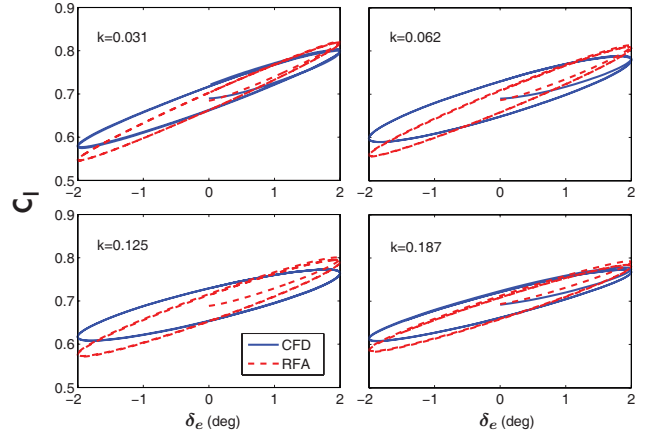Figure 8: Time history of C_l at various reduced frequencies; $A = 2°$, M = 0.6 and $\alpha = 5°$.

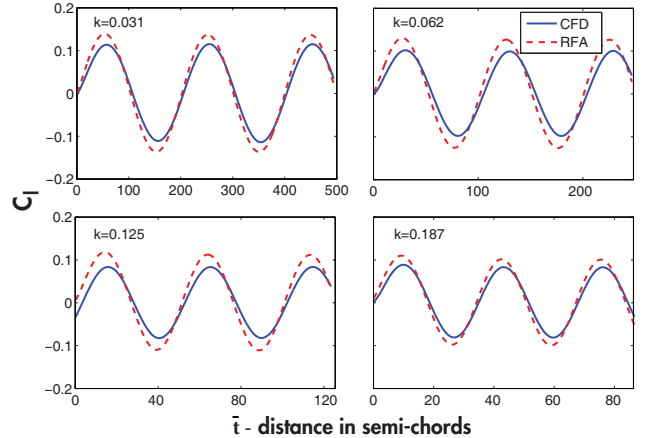Figure 9: Lift C_l versus flap deflection δ_e at various reduced frequencies; $A = 2°$, M = 0.6 and $\alpha = 5°$.

Figure 10: Time history of C_l at various reduced frequencies; $A = 2°$, M = 0.6 and $\alpha = 0°$.
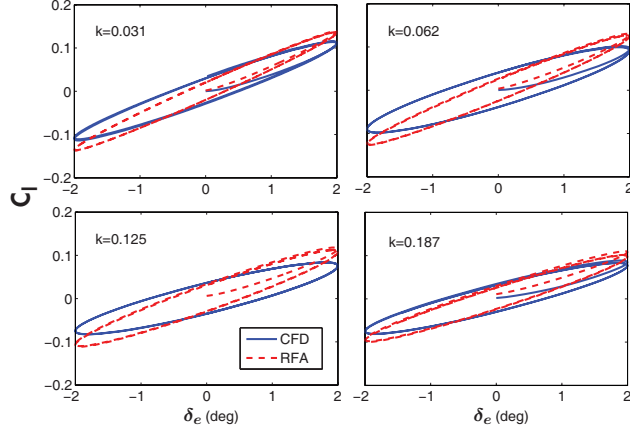
Figure 11: Lift C_l versus flap deflection δ_e at various reduced frequencies; $A = 2°$, M = 0.6 and $\alpha = 0°$.
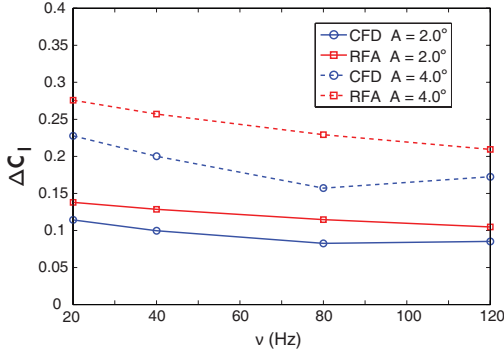

Figure 12: Oscillatory amplitude of lift ΔC_l as a function of flap oscillation frequency; M = 0.6, $\alpha = 5°$, k = 0.031 – 0.187.
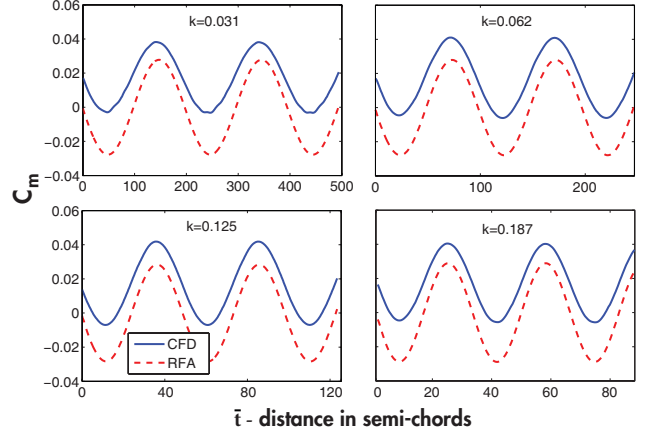

Figure 13: Time history of C_m at various reduced frequencies; $A = 2°$, M = 0.6 and $\alpha = 5°$.

CFD computations oscillates about a non-zero average value of approximately 0.02. The RFA model predicts a zero average value of pitching moment about the quarter-chord point as the result of linear thin-airfoil theory, whereas the CFD based results show non-zero average C_m due to viscous flow effects.

The moment coefficient C_m versus time and flap deflection, at zero incidence $\alpha = 0°$, is shown in Figs. 15 and 16. With $\alpha = 0°$, the offset between the average C_m predicted by RFA and CFD vanishes, due to the symmetry of the flow. The agreement of C_m obtained by the two methods is quite good at $\alpha = 0°$, both in the oscillatory magnitude and the phase lag. This implies that the accuracy of the RFA model is better at smaller airfoil angles of incidence, which is to be expected.

The amplitude of the oscillatory portion of C_m, denoted by ΔC_m, is shown in Fig. 17 for various flap frequencies at flap deflection angles $A = 2°$ and $4°$, and $\alpha = 5°$. For flap deflection angles in this range, the value of ΔC_m varies almost linearly with the amplitude of flap deflection, and increases slightly with flap frequency. The RFA model consistently overestimates the pitching moment due to flap deflection, which resembles the results shown earlier for the lift coefficient. The maximum error in ΔC_m is 34% and the minimum error is 8% for the cases considered.

Results for the hinge moment coefficient C_{hm} plotted versus time and flap deflection δ_e are shown in Figs. 18 and 19, respectively, for $2°$ flap deflection at various frequencies and $\alpha = 5°$. Again, resembling previous results shown for C_m, an offset
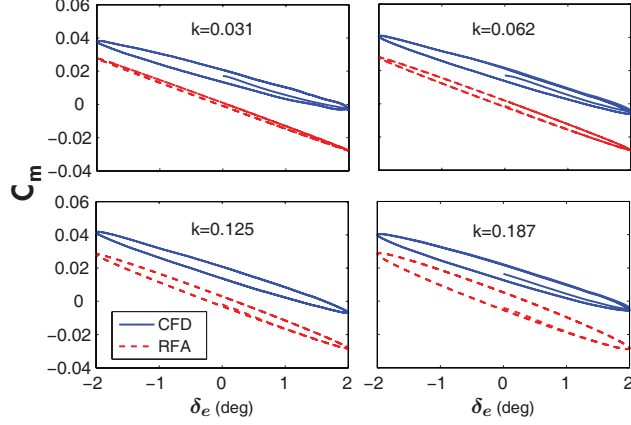
9

Figure 14: Moment C_m versus δ_e at various reduced frequencies; $A = 2°$, $M = 0.6$ and $\alpha = 5°$.
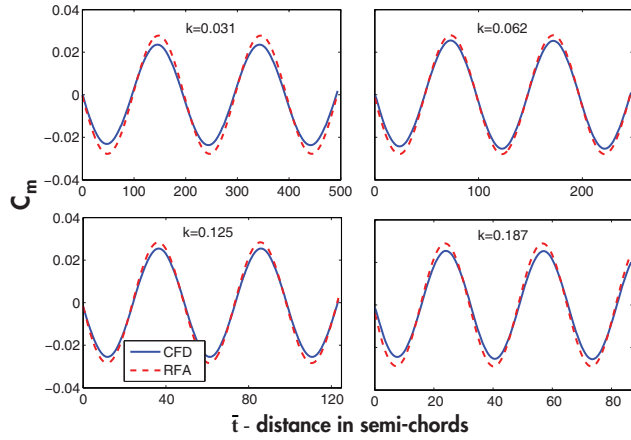

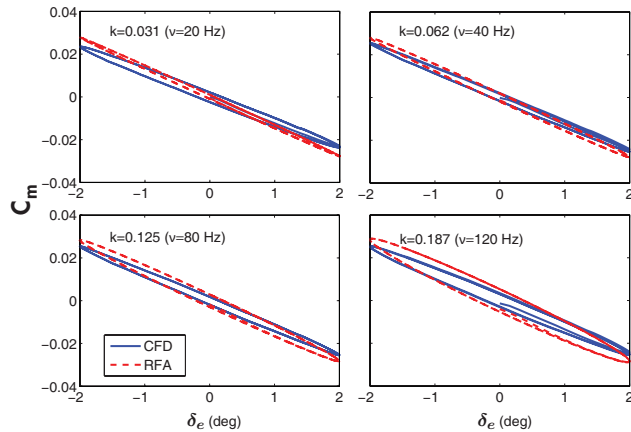Figure 15: Time history of C_m at various reduced frequencies; $A = 2°$, $M = 0.6$ and $\alpha = 0°$.

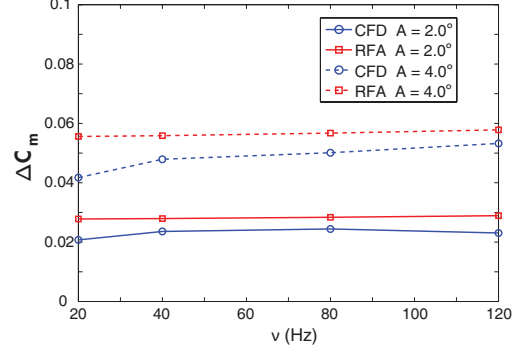Figure 16: Moment C_m versus δ_e at various reduced frequencies; $A = 2°$, $M = 0.6$ and $\alpha = 0°$.

Figure 17: Oscillatory amplitude of pitching moment ΔC_m as a function of flap oscillation frequency; $M = 0.6$ and $\alpha = 5°$.
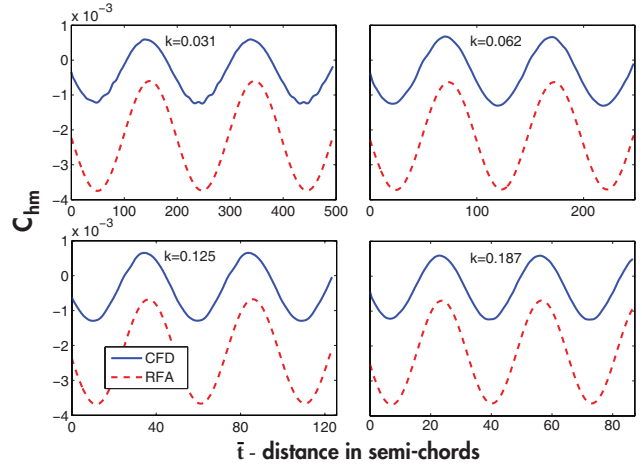

Figure 18: Time history of C_{hm} at various reduced frequencies; $A = 2°$, $M = 0.6$ and $\alpha = 5°$.

exists between the average value of C_{hm} that is obtained from CFD and the RFA model. Figures 20 and 21 show the hinge moment coefficient C_{hm} plotted versus time and flap deflection at zero incidence $\alpha = 0°$. In this case, there is no offset between the average C_{hm} values. The amplitude of the oscillatory component of C_{hm}, denoted by ΔC_{hm} is shown in Fig. 22 for flap deflections of $2°$ and $4°$. These figures indicate that the RFA model significantly overpredicts the hinge moment. This behavior is not surprising because the flap is immersed in relatively thick boundary layers where linear aerodynamic assumptions may not be valid. These findings are also consistent with the conclusions presented in Ref. 21. The maximum error in ΔC_{hm} is 71% and the minimum error is 17% for the cases considered here.
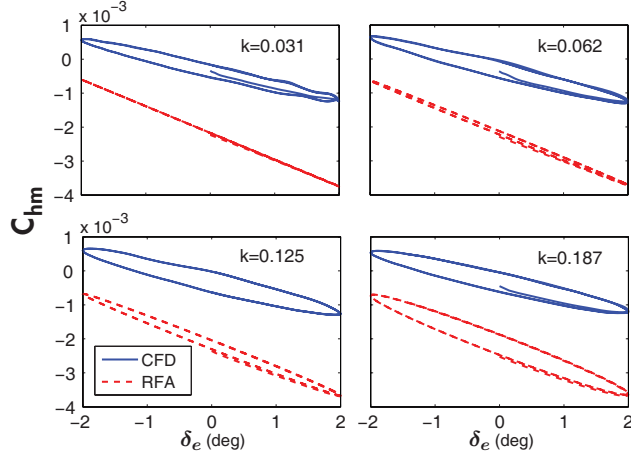
10

Figure 19: Hinge moment C_{hm} versus δ_e at various reduced frequencies; $A = 2°$, $M = 0.6$ and $\alpha = 5°$.
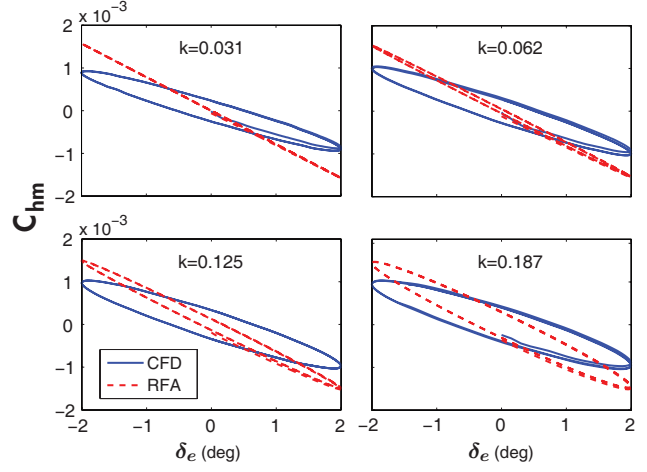

Figure 21: Hinge moment C_{hm} versus δ_e at various reduced frequencies; $A = 2°$, $M = 0.6$ and $\alpha = 0°$.

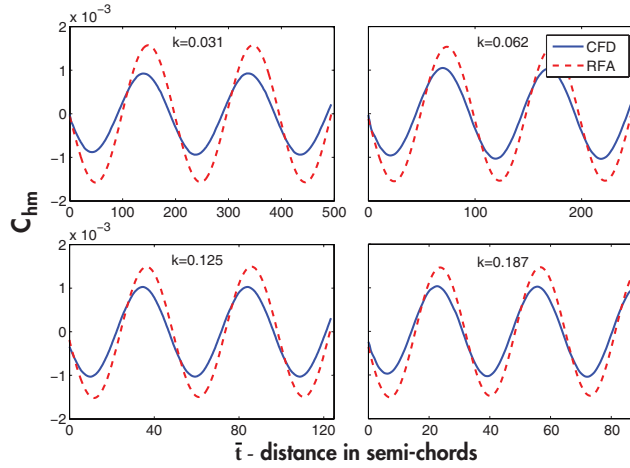Figure 20: Time history of C_{hm} at various reduced frequencies; $A = 2°$, $M = 0.6$ and $\alpha = 0°$.

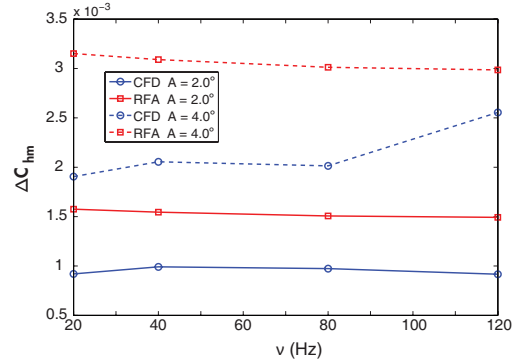Figure 22: Oscillatory component of hinge moment ΔC_{hm} as a function of flap oscillation frequency; $M = 0.6$ and $\alpha = 5°$.
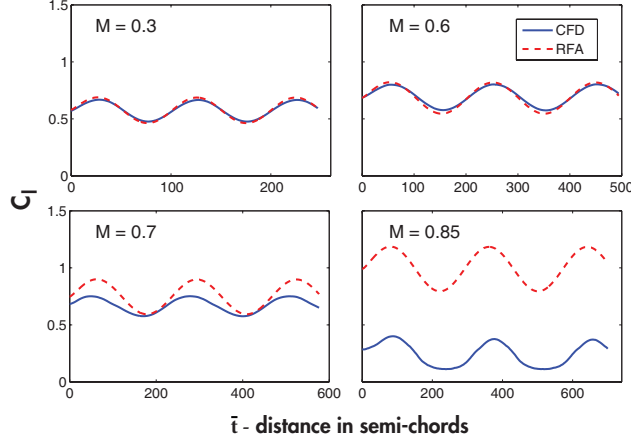
11

Figure 23: Time history of C_l at various Mach numbers; $A = 2°$, $k = 0.031$, and $\alpha = 5°$.

Effect of freestream Mach number

The effect of free stream Mach number on the accuracy of the predicted unsteady airloads is considered next. Four different values of the free stream Mach number are chosen, namely, M = 0.3, 0.6, 0.7, and 0.85. Time history of the lift coefficient C_l is shown in Fig. 23 for 2° flap deflection at reduced frequency $k = 0.031$. At this airfoil incidence angle, $\alpha = 5°$, the agreement in C_l between the two models is reasonable until M=0.7, after which the discrepancy between the two approaches becomes quite large. At M=0.85 the RFA model predicts a C_l value that is three times larger than the CFD prediction.
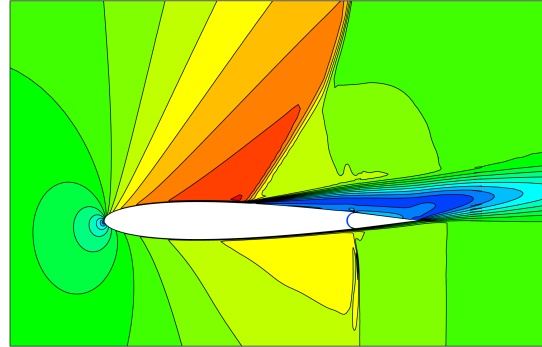
Snapshots of Mach contours of the flow over a NACA0012 airfoil at the instant when $\delta_e = 0°$ are shown in Fig. 24 for $M = 0.7$ and 0.85. A strong shock on the airfoil ahead of the flap is evident for the $M = 0.85$ case and it produces massive shock-induced boundary layer separation as can be seen in Fig. 24. The RFA model is not suitable for predicting airloads at such flow conditions.

Drag due to flap deflection

Drag has an important practical role in the implementation of ACF for rotorcraft, and the accurate prediction of drag is essential for rotor performance considerations. Drag predictions from the simple drag correction given by Eq. (8), the CFD++ code, as well as a CFD based surrogate drag model, are presented in this section. Drag predictions from the
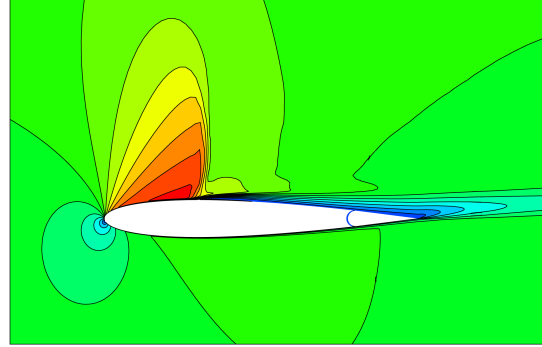
(a) M = 0.7

(b) M = 0.85

Figure 24: Snapshots of Mach contours of the unsteady flow over the NACA0012 airfoil; $\alpha = 5°$ and $\delta_e = 0°$.

12

simple drag correction and the CFD code are evaluated and compared first, followed by the results from the CFD based surrogate drag model.

Simple drag correction

Drag coefficients C_d obtained from the simple drag model and CFD are plotted in Fig. 25, for the case of $\alpha = 5°$ and flap deflection $A = 2°$ at various frequencies. A similar comparison of the drag coefficients is also shown in Fig. 26, for the same conditions as in Fig. 25 except for an incidence angle of $\alpha = 0°$.

It is evident from Figs. 25 and 26 that predictions from the drag model, Eq. (8), differ substantially from the CFD results. The simple drag model underpredicts the oscillatory drag at $\alpha = 5°$ and overestimates it at $\alpha = 0°$. Furthermore, it is interesting to note that for the case of $\alpha = 5°$, as shown in Fig. 25, the drag predicted by the simple model appears to oscillate twice as fast (or twice as many times) as the unsteady drag predicted by CFD. However, this difference in the number of oscillation does not occur for $\alpha = 0°$, as can be seen from Fig. 26. This behavior is explained by recognizing the fact that the absolute value of δ_e used in Eq. (8) implies that flap deflections are always assumed to produce a drag penalty in the simple drag model. At $\alpha = 0°$ the drag increases during both upward and downward strokes of the flap, as can be expected from the symmetric mean flow and predicted by both the simple model and CFD. The drag still increases for the downward flap stroke at $\alpha = 5°$; however, it is reduced when the flap deflects upward, as indicated by the CFD computations. This reduction in drag is due to the decreased boundary layer thickness on the upper surface of the airfoil, while the flap deflects upward. Such dissimilar effects of flap deflection on C_d are illustrated in Fig. 27 where unsteady drag C_d is plotted against flap deflection angles, at both $\alpha = 0°$ and $5°$. The simple drag model is clearly an oversimplification of the drag due to flap deflections, in particular when viscous effects are significant.

The drag responses at various flap reduced frequencies from the CFD calculations are shown in Figs. 28 and 29. The C_d versus δ_e curve in Fig. 29 exhibits a butterfly shape, different from Fig. 28, due to the reason explained earlier. The drag responses shown in Fig. 29 for the $\alpha = 0°$ have been filtered to eliminate high frequency variations that may be associated with the non-conservation condition at the overset mesh boundaries which assumes a more significant role at smaller drag values near
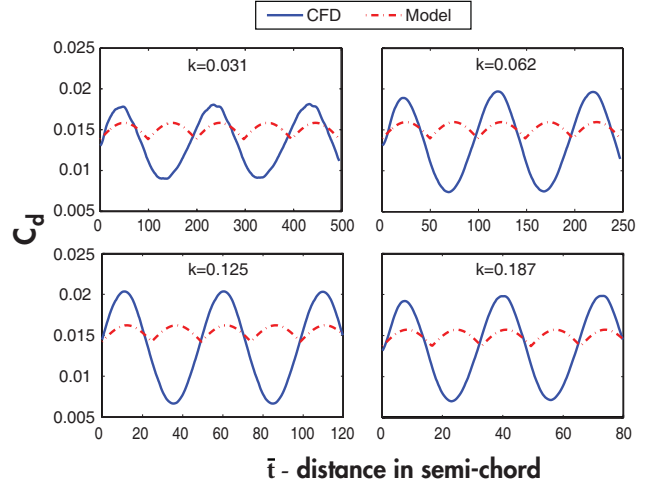

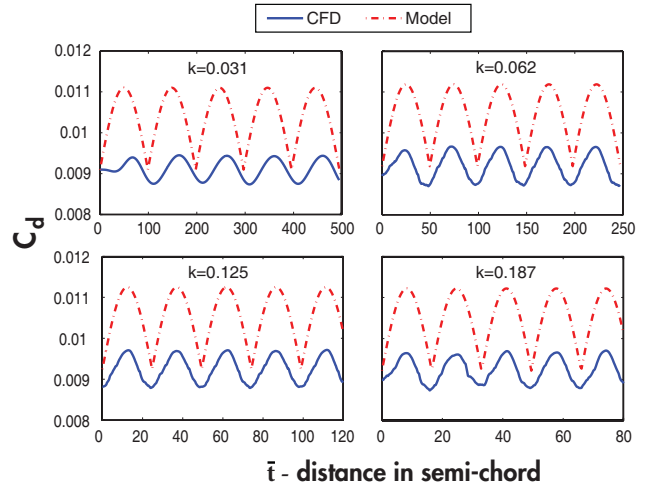Figure 25: Time history of C_d at various reduced frequencies; M = 0.6, $\alpha = 5°$, and $A = 2°$.

Figure 26: Time history of C_d at various reduced frequencies; M = 0.6, $\alpha = 0°$, and $A = 2°$.

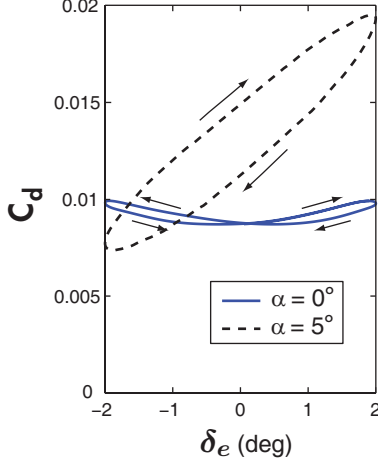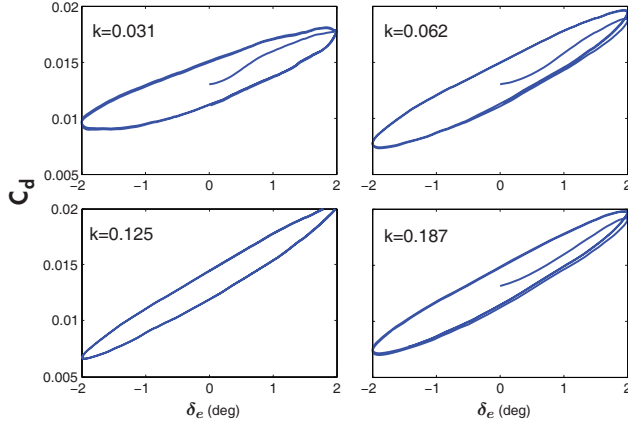Figure 27: C_d versus δ_e for $\alpha = 0°$ and $5°$; M = 0.6 and k = 0.062.

Figure 28: C_d versus δ_e at various reduced frequencies; $A = 2°$, M = 0.6 and $\alpha = 5°$.

zero incidence angle.

CFD based surrogate drag model

Since the simplified drag model represented by Eq. (8) is inaccurate, a new CFD based drag model has been developed, so as to enable one to predict drag penalty associated with active flaps in a more reliable manner. The new drag model was constructed using a surrogate based approach described earlier. The fitting ranges of the three design variables for which the surrogate based drag model is generated, namely M, α, and δ_e, are given below

$$0.2 \leq M \leq 0.95$$
$$-10° \leq \alpha \leq 30°$$
$$-5° \leq \delta_e \leq 5°$$

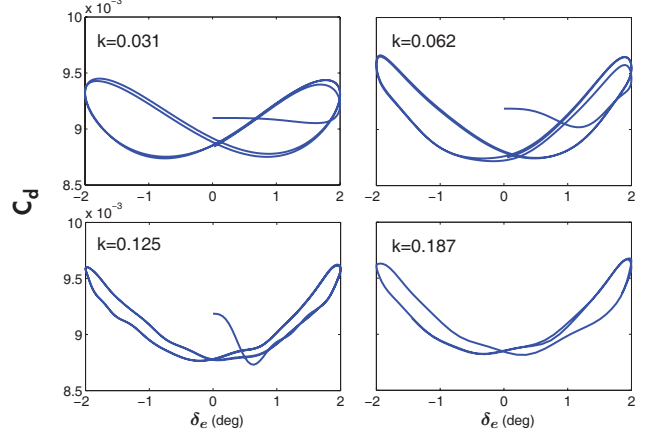Figure 29: C_d versus δ_e for $A = 2.0°$ at various reduced frequencies; M = 0.6 and $\alpha = 0°$.

The range of parameters encompasses all practical flow conditions encountered by an active flap system in rotorcraft applications. A smaller parameter range may also be considered for constructing the drag surrogate, and therefore it will require less computational effort to generate. However, it will be limited in its range of applicability. In this study, a total number of 3000 fitting points are generated using Optimal Latin Hypercube (OLH) sampling technique [36]. The CFD++ code was then used to obtain converged drag solutions at the flow conditions defined by these 3000 points, employing parallel computations. Subsequently, kriging is used to generate the drag surrogate for these sampling data. In order to quantify the accuracy of the surrogates, an additional 300-point OLH space was generated as testing points at which the errors of the surrogate predictions were evaluated against direct CFD computations (true responses). The absolute errors are defined by

$$\varepsilon_i^{(tp)} = \frac{|y^{(i)} - \hat{y}^{(i)}|}{\bar{y}} \qquad (11)$$

The average and maximum errors are

$$\varepsilon_{\text{avg}}^{(tp)} = \frac{\sum_{i=1}^{N_{tp}} \varepsilon_i^{(tp)}}{N_{tp}} \qquad (12)$$

$$\varepsilon_{\text{max}}^{(tp)} = \text{Max}\left\{\varepsilon_1^{(tp)}, \ldots, \varepsilon_{N_{tp}}^{(tp)}\right\} \qquad (13)$$

At these 300 test points, the surrogate drag model generated with the 3000 fitting points has an average error of 1.7%, while the maximum error is 19.5%. The small average error for the surrogate in-
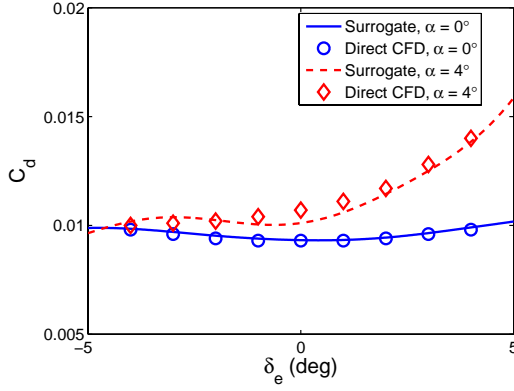
Figure 30: Variation of drag to flap deflection for NACA0012 airfoil with a 20%c flap; $\alpha = 0°$ and $5°$, $M = 0.6$.
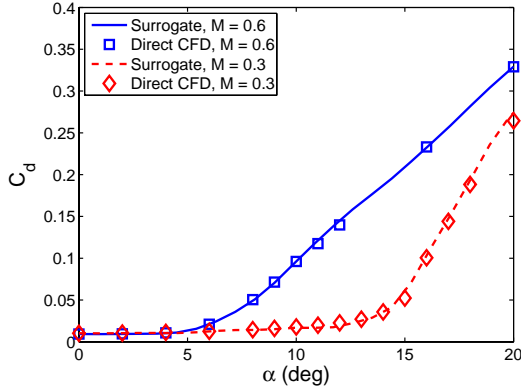

Figure 31: Drag polars for NACA0012 airfoil without flap deflection; $\delta_e = 0°$, $M = 0.3$ and 0.6.

dicates that the model is very accurate over the entire range of interest. Next, the surrogate is used to generate drag plots at specific flow conditions to further examine the accuracy of the surrogate model. First the variation of drag against flap deflection δ_e is shown in Fig. 30, for two airfoil incidence angles $\alpha = 0°$ and $\alpha = 4°$, at Mach number of 0.6. The predictions of the surrogate model are shown in the figure by the solid and dashed lines, along with direct CFD calculations indicated by the circle and diamond symbols. The surrogate model accurately predicted the drag variation at both airfoil incidence angles. For further comparison, the drag polars are also shown in Fig. 31, for zero flap deflection. The surrogate model compares very well with the drag polars calculated by the CFD code.

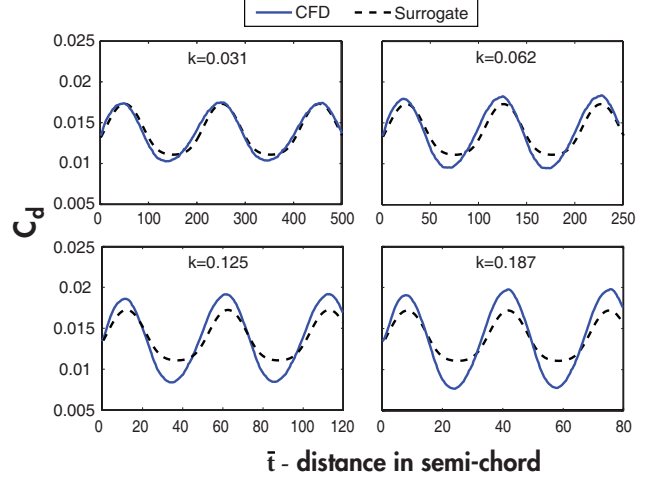The surrogate drag model was generated from CFD drag predictions at steady flow conditions,

Figure 32: Time history of C_d at various reduced frequencies; $A = 2°$, $M = 0.6$ and $\alpha = 5°$.

therefore this model only accounts for drag in a quasisteady manner. Comparisons of drag obtained from this model to fully unsteady drag computed by CFD are shown in Figs. 32 and 33. Compared to the results obtained using the simple drag model, as given earlier in Figs. 25 and 26, the surrogate model clearly represents a significant improvement. Note that the surrogate model also predicts the same number of oscillation as the CFD predictions, for both $\alpha = 0°$ and $5°$. However, the surrogate drag model also substantially underpredicts the magnitudes of unsteady drag, particularly at higher reduced frequencies. This implies that flow unsteadiness needs to be taken into account for future studies.

Concluding Remarks

Two-dimensional unsteady airloads due to oscillating flap motion predicted by the Rational Function Approximation (RFA) model are compared with CFD based calculations. The comparison was conducted for a representative range of flow conditions and combinations of parameters such as the airfoil angle of attack, flap deflection amplitudes, reduced frequencies and freestream Mach numbers.

The RFA model consistently overestimates unsteady lift, moment, and in particular hinge moment, which is attributed to viscous effects, nonlinearity, thickness, and possibly the hinge gap that is modeled only in the CFD approach. The discrepancy between the RFA and CFD predictions
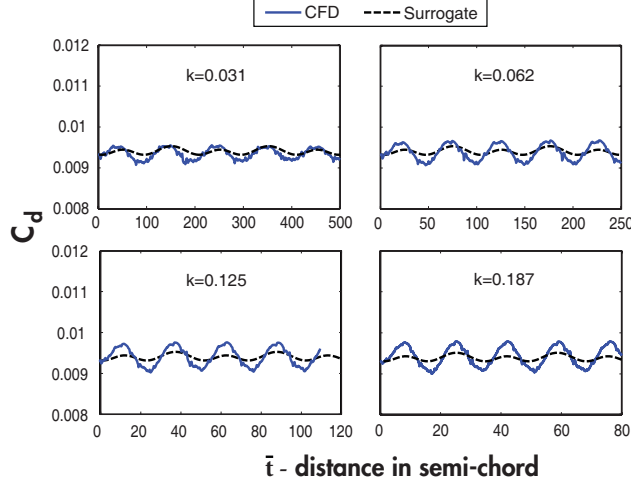
Figure 33: Time history of C_d at various reduced frequencies; $A = 2°$, M $= 0.6$ and $\alpha = 0°$.

increases at high Mach numbers, i.e. $M > 0.7$. Overall, the oscillatory components of the unsteady airloads are reasonably well captured for most cases considered in this study, thus establishing the validity of the RFA model for its use in comprehensive rotorcraft simulation codes and preliminary design trend studies. Furthermore, the overall accuracy of the RFA model can be improved by introducing empirical coefficients, as is done also in Leishman's model [10].

A simplified drag model, Eq. (8), used in earlier studies to account for additional drag due to flap motion was found to be inaccurate. Therefore, a surrogate based drag model was developed and shown to be capable of improved drag predictions. This new improved model will facilitate future studies involving the evaluation of performance penalty associated with active flaps.

It is important to note that despite its relative simplicity, the RFA model provides a good estimate of unsteady effect of the trailing-edge flap, at Mach numbers below 0.70 and the reduced frequency range representative of practical implementation for vibration reduction. The applicable Mach number range depends also on the airfoil incidence angle and magnitude of flap deflection. The estimates are good in the case of smaller mean airfoil angles of incidence and smaller flap deflections. Compared to the CFD approach, the computational efficiency of the RFA approach provides a distinct advantage for computationally intensive applications such as rotorcraft simulations with active control.

REFERENCES

1. Friedmann, P. P. , de Terlizzi, M. , and Myrtle, T. F. , "New Developments in Vibration Reduction with Actively Controlled Trailing Edge Flaps," *Mathematical and Computer Modelling*, Vol. 33, 2001, pp. 1055–1083.

2. Friedmann, P. P. and Millott, T. A. , "Vibration Reduction in Rotorcraft Using Active Control: A Comparison of Various Approaches," *Journal of Guidance, Control, and Dynamics*, Vol. 18, (4), July-August 1995, pp. 664–673.

3. Millott, T. A. and Friedmann, P. P. , "Vibration Reduction in Helicopter Rotors Using an Actively Controlled Partial Span Trailing Edge Flap Located on the Blade," NASA-CR-4611, June 1994.

4. Milgram, J. H. and Chopra, I. , "Helicopter Vibration Reduction with Trailing Edge Flaps," Proceedings of the 36th AIAA/ASME/ASCE/AHS/ASC Structures, Structural Dynamics and Materials Conference, New Orleans, La., 1995.

5. Myrtle, T. F. and Friedmann, P. P. , "Application of a New Compressible Time Domain Aerodynamic Model to Vibration Reduction in Helicopters Using an Actively Controlled Flap," *Journal of the American Helicopter Society*, Vol. 46, (1), January 2001, pp. 32–43.

6. de Terlizzi, M. and Friedmann, P. P. , "Active Control of BVI Induced Vibrations Using a Refined Aerodynamic Model and Experimental Correlation," American Helicopter Society 55th Annual Forum Proceedings, Montreal, Canada, May 25-27 1999, pp. 599–615.

7. Straub, F. K. , Kennedy, D. K. , Stemple, A. D. , Anand, V. R. , and Birchette, T. S. , "Development and Whirl Tower Test of the SMART Active Flap Rotor," Proceedings of SPIE: Smart Structures and Materials 2004, Vol. 5388, July 2004, pp. 202–212.

8. Patt, D. , Liu, L. , and Friedmann, P. P. , "Simultaneous Vibration and Noise Reduction in Rotorcraft Using Aeroelastic Simulation," *Journal of the American Helicopter Society*, Vol. 51, (2), April 2006.

9. Roth, D. , "Advanced Vibration Reduction by IBC Technology," 30th European Rotorcraft Forum, Marseille, France, September 14-16, 2004.

10. Hariharan, N., and Leishman, J.G., "Unsteady Aerodynamics of a Flapped Airfoil in Subsonic Flow by Indicial Concepts," *Journal of Aircraft*, Vol. 33, (5), September-October 1996, pp. 855 – 868.

11. Rogers, K. L. , Airplane Math Modeling Methods for Actively Control Design. AGARD-CP-228, August 1977.

12. Edwards, J. H. , "Application of Laplace Transform Methods to Airfoil Motion and Stability Calculations," Proceedings of the 20th Structures, Structural Dynamics and Materials Conference, St. Louis, MO, April 1979. AIAA Paper No. 1979-772.

13. Karpel, M. , Design for Active and Passive Flutter Suppression and Gust Alleviation. NASA-CR-3492, November 1981.

14. Vepa, R. , Finite State Modeling of Aeroelastic Systems. NASA-CR-2779, 1977.

15. Depailler, G. and Friedmann, P. P. , "Reductions of Vibrations Due to Dynamic Stall in Helicopters Using an Actively Controlled Flap," Proceedings of the 43rd AIAA/ASME/ASCE/AHS/ACS Structures, Structural Dynamics and Materials Conference, Denver, CO, April 2002. AIAA Paper No. 2002-1431.

16. Liu, L. , Friedmann, P. P. , Kim, I. , and Bernstein, D. , "Vibration Reduction and Performance Enhancement in Rotorcraft Using Actively Controlled Flaps," Proceedings of the 62nd American Helicopter Society Annual Forum, Phoenix, May 2006.

17. Patt, D. , Liu, L. , and Friedmann, P. P. , "Rotorcraft Vibration Reduction and Noise Prediction Using a Unified Aeroelastic Response Simulation," *Journal of the American Helicopter Society*, Vol. 50, (1), January 2005, pp. 95–106.

18. Carpenter, M. , Singer, B. , Yamaleev, N. , Vatsa, V. , Viken, S. , and Atkins, H. , "The Current Status of Unsteady CFD Approaches for Aerodynamic Flow Control," AIAA Paper 2002-3346, St. Louis, MO, June 2002.

19. Bartels, R. and Schuster, D. , "Comparison of Two Navier-Stokes Methods with Benchmark Active Control Technology Experiments," *Journal of Guidance, Control, and Dynamics*, Vol. 23, (6), November-December 2000, pp. 1094–1099.

20. Scott, R. , Hoadley, S. , Wieseman, C. , and Darham, M. , "Benchmark Active Controls Technology Model Aerodynamic Data," *Journal of Guidance, Control, and Dynamics*, Vol. 23, (5), September-October 2000, pp. 914–921.

21. Roughen, K. , Baker, M. , and Fogarty, T. , "Computational Fluid Dynamics and Doublet-Lattice Calculation of Unsteady Control Surface Aerodynamics," *Journal of Guidance, Control, and Dynamics*, Vol. 24, (1), January 2001, pp. 160–166.

22. van Dam, C. , "Recent Experience with Different Methods of Drag Prediction," *Progress in Aerospace Sciences*, Vol. 35, (8), November 1999, pp. 751–798.

23. Vassberg, J. , Tinoco, E. , Mani, M. , Brodersen, O. , Eisfeld, B. , Wahls, R. , Morrison, J. , Zickuhr, T. , Laflin, K. , and Mavriplis, D. , "Summary of the Third AIAA CFD Drag Prediction Workshop," AIAA Paper No. 2007-0260, Reno, NV, January 2007.

24. Rodden, W. P. and Albano, E. , "A Doublet-Lattice Method for Calculating Lift Distributions on Oscillating Surfaces in Subsonic Flows," *AIAA Journal*, Vol. 7, 1969, pp. 279–285.

25. Bisplinghoff, R. L. , Ashley, H. , and Halfman, R. , Aeroelasticity, Addison-Wesley, 1955, Ch. 6, pp. 317–325.

26. Peroomian, O. , Chakravarthy, S. , Palaniswamy, S. , and Goldberg, U. , "Convergence Acceleration for Unified-Grid Formulation Using Preconditioned Implicit Relaxation," AIAA Paper 98-0116, Reno, NV, January 1998.

27. Peroomian, O. , Chakravarthy, S. , and Goldberg, U. , "A "Grid-Transparent" Methodology for CFD," AIAA Paper 97-0724, Reno, NV, January 1997.

28. Spalart, P. and Allmaras, S. , "A One-Equation Turbulence Model for Aerodynamic Flows," *La Recherche Aérospatiale*, Vol. 1, 1994, pp. 5–21.

29. Shih, T. , "Overset Grids: Fundamentals and Practical Issues," AIAA Paper No. 2002-3259, St. Louis, MO, June 2002.

30. Sacks, J. , Welch, W. J. , Mitchell, T. J. , and Wynn, H. P. , "Design and Analysis of Computer Experiments," *Statistical Science*, Vol. 4, (4), (4), 1989, pp. 409–435.

31. Martin, J. and Simpson, T. , "Use of Kriging Models to Approximate Deterministic Computer Models," *AIAA Journal*, Vol. 43, (4), April 2005, pp. 853–863.

32. Jones, D. R. , "A Taxonomy of Global Optimization Methods Based on Response Surfaces," *Journal of Global Optimization*, Vol. 21, 2001, pp. 345–383.

33. Sasena, M. , "Flexibility and Efficiency Enhancements for Constrained Global Optimization with Kriging Approximations," Ph.D. Dissertation, University of Michigan, 2002. Mechanical Engineering.

34. Lophaven, S. N. , Nielsen, H. B. , and Søndergaard, J. , A Matlab Kriging Toolbox, Version 2.0. Informatics and Mathematical Modeling, DTU, 2002. Technical Report IMM-TR-2002-12.

35. Landon, R. H. , Compendium of Unsteady Aerodynamic Measurements - NACA0012 Oscillatory and Transient Pitching. AGARD-R-702, 1982.

36. Queipo, N. V. , Haftka, R. T. , Shyy, W. , Goel, T. , Vaidyanathan, R. , and Tucker, P. K. , "Surrogate-Based Analysis and Optimization," *Progress in Aerospace Sciences*, Vol. 41, 2005, pp. 1–28.